Engineering Ni/Ni₃N/MoN interface with strain modulation toward sustainable high current density alkaline seawater hydrogen production via in situ ammonnium formation

Zhiquan Yang,[a, c] Kunfeng Zhao,[a] Chenhao Shi,[a, b] Jing Zhou,[d] Dingwang Yuan[d,] and Zhiguo Yi,[a, b, c,] *

[a] State Key Lab of High Performance Ceramics, Shanghai Institute of Ceramics, Chinese Academy of Sciences, Shanghai 200050, PR China.

[b] Center of Materials Science and Optoelectronics Engineering, University of Chinese Academy of Sciences, Beijing 100049, PR China

[c] School of Microelectronics, Shanghai university, Shanghai 201800, PR China.

[d] College of Materials Science and Engineering, Hunan university, Changsha 410082, PR China.

*Corresponding authors

E-mail addresses: zhiguo@mail.sic.ac.cn (Zhiguo Yi)

Keywords: Interface Engineering, Strain Effect, Transition Metal Nitrides, Hydrogen Evolution Reaction, In Situ Ammonium Formation, Seawater Electrolysis.

Materials

All chemicals were of analytical grade without further purification. Nickel Chloride ($NiCl_2$), ammonium chloride (NH_4Cl), potassium hydroxide (KOH), D-(+)-Glucose ($C_6H_{12}O_6$) and sodium molybdate dihydrate ($Na_2MoO_4 \cdot 2H_2O$) were purchased from Shanghai Titan Scientific Co. Ethanol absolute (C_2H_6O) and acetone (C_3H_6O) were bought from Shanghai Lingfeng Chemical Reagent Co. Hydrochloric acid (HCl) was obtained from Sinopharm Reagent Co. Seawater was stem from Bohai Bay, China.

Electrochemical Tests

All the electrochemical experiments were implemented on an electrochemical station (ZAHNER ZenNium-XC). A three-electrode setup was employed with a standard Hg/HgO electrode as the reference electrode, a Pt sheet as the counter electrode, the prepared-electrocatalyst functioned as the working electrode, 1 M KOH and 1 M KOH natural seawater as the electrolyte. The loading mass of NN/NF, MN/NF, NN/MN/NF is 36.9 mg cm^{-2}, 2.5 mg cm^{-2} and 40.3 mg cm^{-2}, respectively. The natural seawater from Bohai Bay, China. Linear sweep voltammetry (LSV) measurement was conducted at a scan rate of 2 mV s^{-1}. Presented potentials were converted to reversible hydrogen electrode (RHE) based on the equation: $E_{RHE} = E_{Hg/HgO} + 0.098 + 0.059 \times pH$. The LSV measurement results were fitted and calculated to obtain the Tafel slope. The equation formula of the Tafel curves is: $\eta = a + b \times \log|j|$. η represents the overpotential (RHE), b represents the Tafel slope and j is the current density. Electrochemical impedance spectroscopy (EIS) was measured from 10^{-1} to 10^5 Hz with an amplitude of 5 mV. Cyclic voltammetry (CV) experiments were conducted in non-Faradic current region with different scanning rates from 10 to 50 mV s^{-1} to determine the double layer capacitances (C_{dl}) values of the studied catalysts. The stability of NN/MN/NF were conducted adopting chronopotentiometry I-t measurement in different solutions at room temperature. The dynamic potential polarization curves (PDP) were obtained over a voltage range of ±500 mV around the open-circuit voltage.

Turnover Frequency (TOF) calculation

Provided that all catalytically active surface sites are fully accessible to the solution, the TOF is evaluated as: $TOF = j/(2Fn)$, in which j denotes the HER current density, n represents the number of active sites, and F is Faraday constant (96485 C mol^{-1}). The site number n was quantified by CV acquired between 0 and 0.6 V vs. RHE at 50 mV s^{-1} in 1.0 M KOH. The surface charge density (Q_s) was obtained by integrating each voltammogram. Subsequently, the n was subsequently calculated via $n = Q_s/F$

Identification and quantification of the products

The generated amount of H_2 evolved at the cathode was quantified using the water-drainage method. The

Faradaic efficiency for H_2 production was calculated according to FE (H_2) = 2Fn/Q × 100%. Where F denotes the faraday constant (96485 C mol^{-1}), n is the amount of H_2 generated (mol), Q represents the total charge passed (C).

Electrochemical measurements in the AEMWE

An AEMWE system was utilized to assess the industrial applicability of the prepared catalysts. The AEMWE consists of a cathode, an anode, an anion exchange membrane, a gas diffusion layer, and graphite/titanium end plates with serpentine flow channels. The self-standing NN/NF, MN/NF and NN/MN/NF served as the cathode, while NiFeLDH/NF functioned as the anode. The membrane was activated by immersing in a 1 M KOH solution at room temperature for 24 h. During the experiments, 1 M KOH was circulated at a flow rate of 3 mL min^{-1} using a peristaltic pump. Subsequently, polarization curves were recorded by measuring the cell voltage across increasing current densities at a scan rate of 5 mV s^{-1}. The extended stability of electrolyzer was evaluated via chronoamperometry testing under specific conditions.
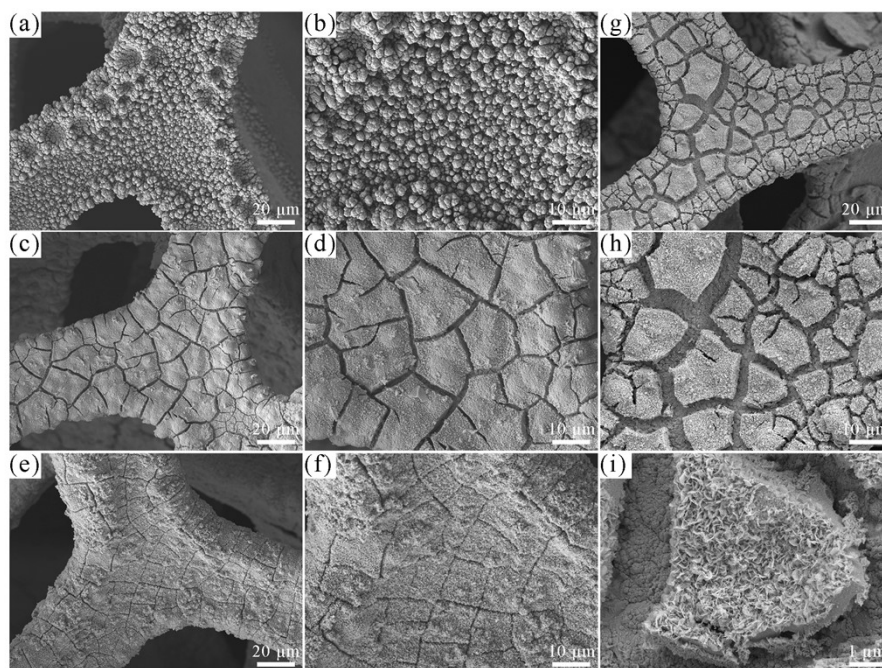

Figure S1 SEM images of a-b) Ni/NF c-d) Ni/Ni(OH)$_2$/NF. e-f) Ni/Ni(OH)$_2$/MoO$_2$/NF. g-i) NN/MN/NF.
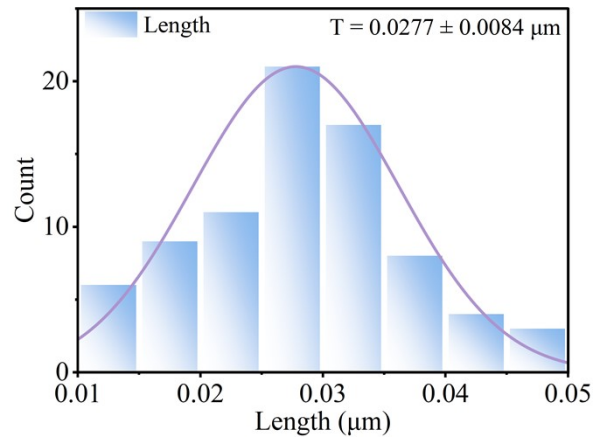
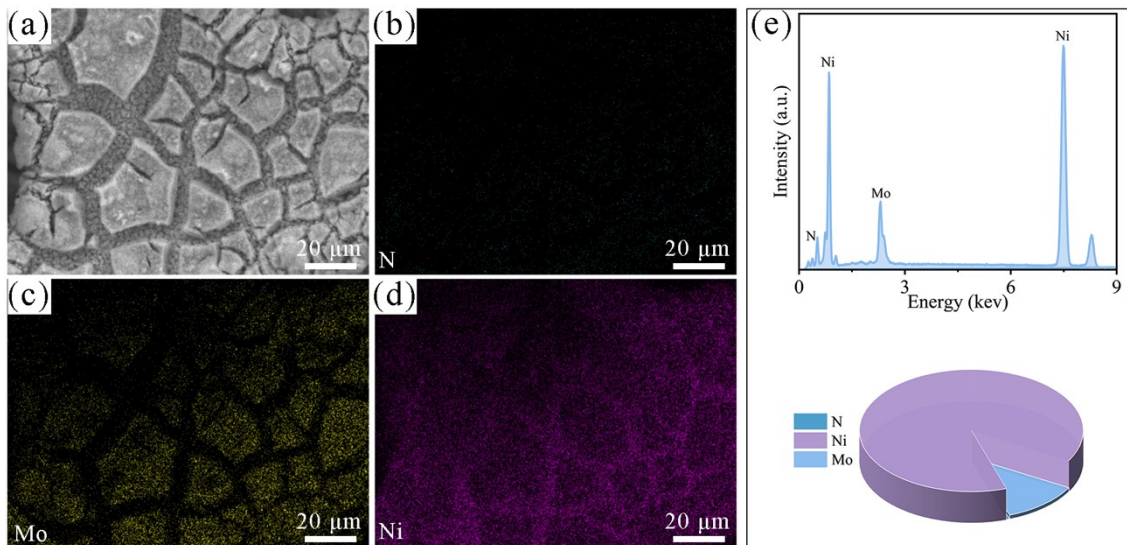**Figure S2** The average thickness of MoO$_2$ nanosheets.

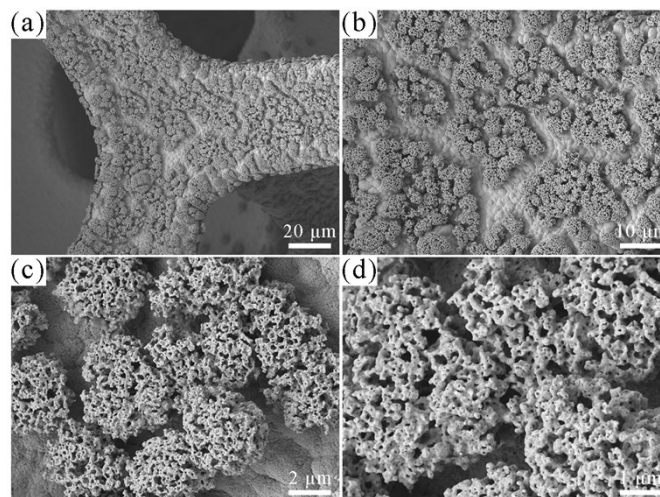**Figure S3** a-g) SEM images and corresponding EDS analysis of NN/MN/NF.

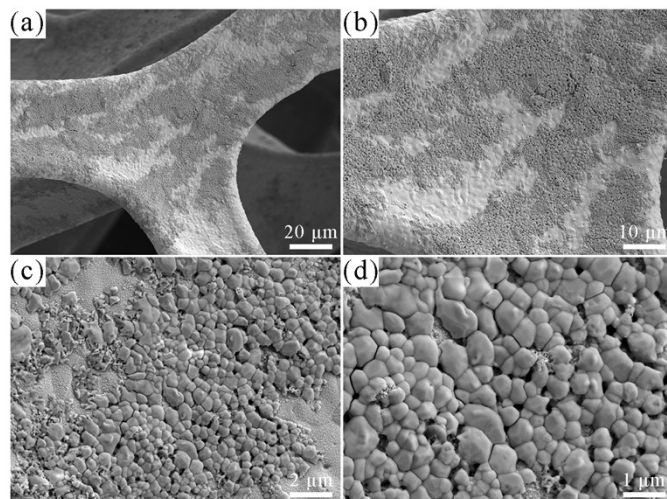

Figure S4 a-d) SEM images of NN/NF.

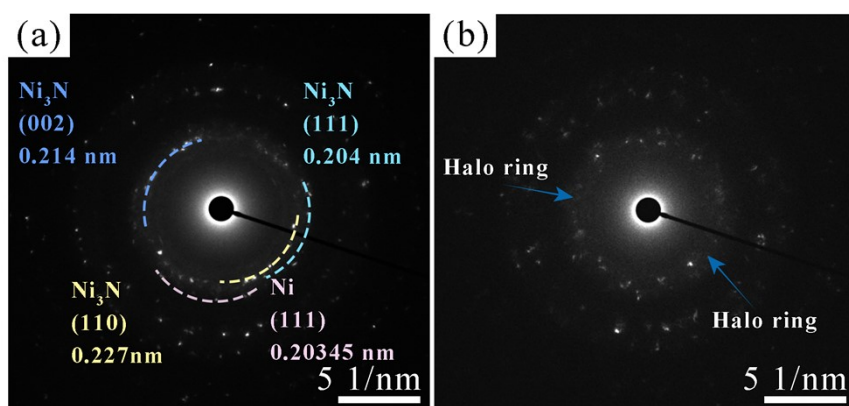**Figure S5** a-d) SEM images of MN/NF.

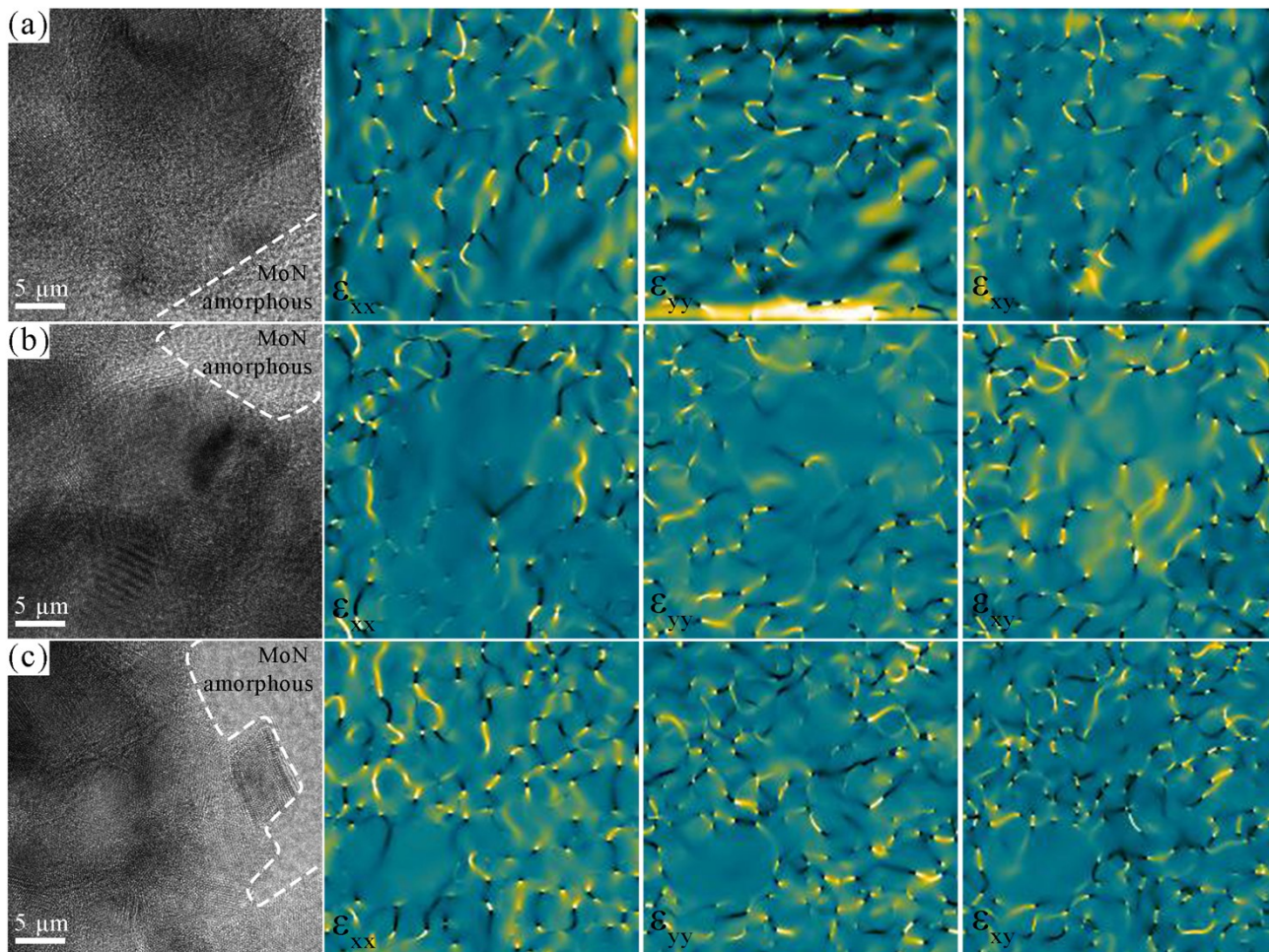
Figure S6 SAED patterns of NN/MN/NF.

Figure S7 a-c) High-resolution TEM images and strain distributions of NN/MN.
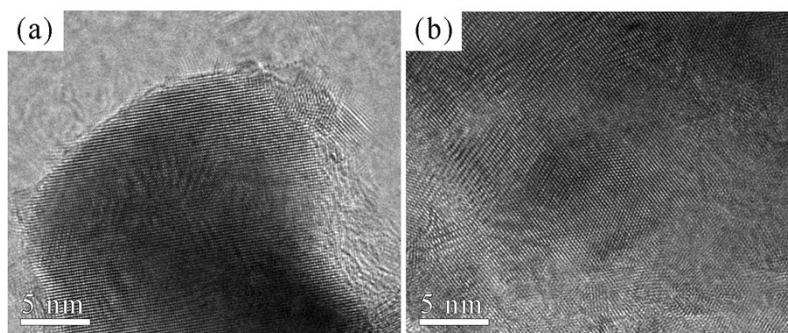

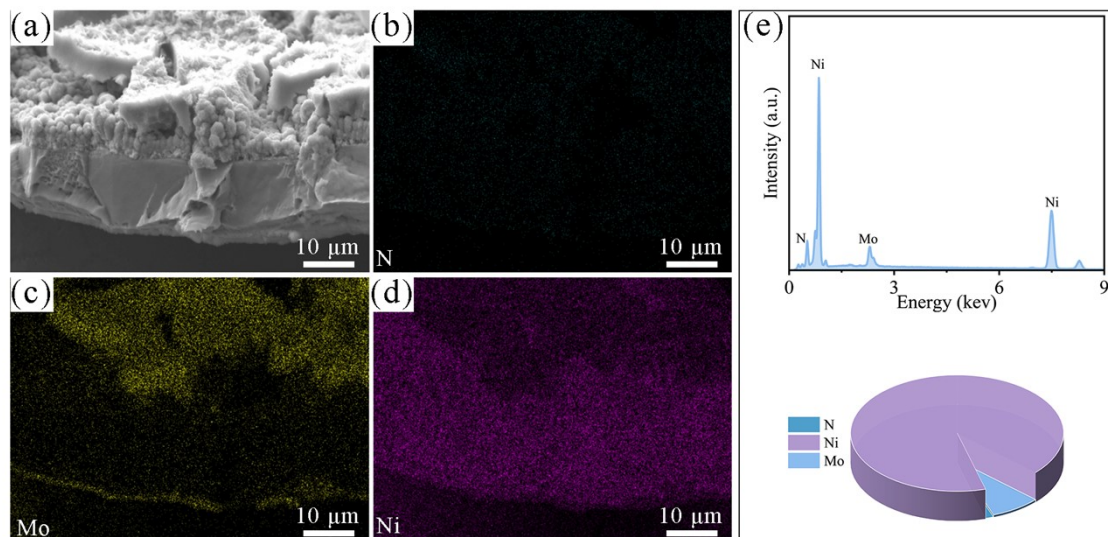**Figure S8** High-resolution TEM images of NN.

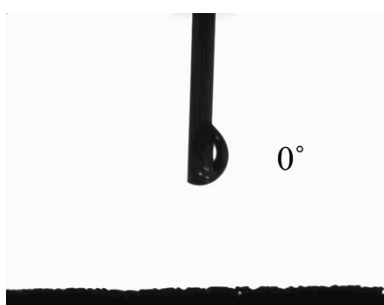**Figure S9** The cross-section SEM image and EDS mapping of the NN/MN/NF.

Figure S10 Contact angle of NN/MN/NF.

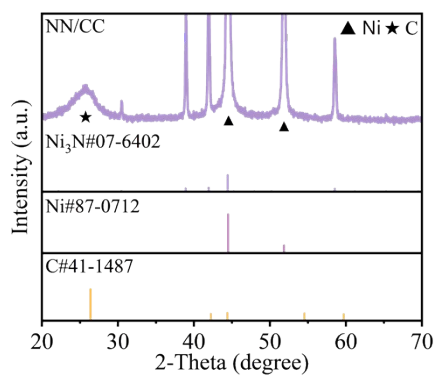**Figure S11** XRD analysis of NN/CC.
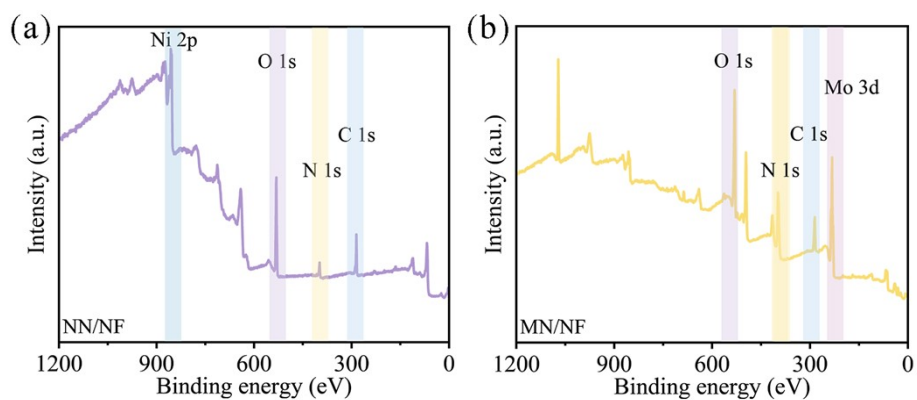
Figure S12 XPS survey spectra of a) NN/NF. b) MN/NF.

Figure S13 CV curves of a) NF. b) NN/NF. c) MN/NF. d) NN/MN/NF in 1 M KOH at 0.33-0.43 V vs RHE with the non-Faradaic potential regions from 10-50 mV s^{-1}.
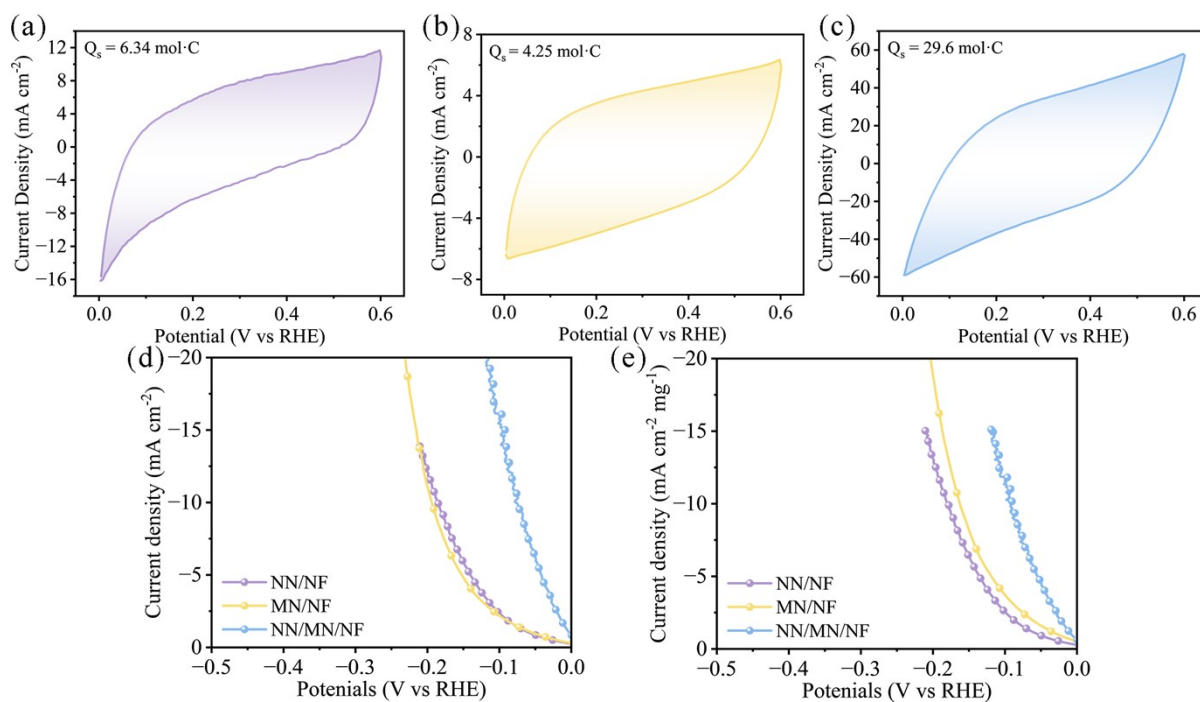
Figure S14 a-c) Q_s of NN/NF, MN/NF and NN/MN/NF, respectively. d) TOFs and e) mass activity of all samples in 1 M KOH.
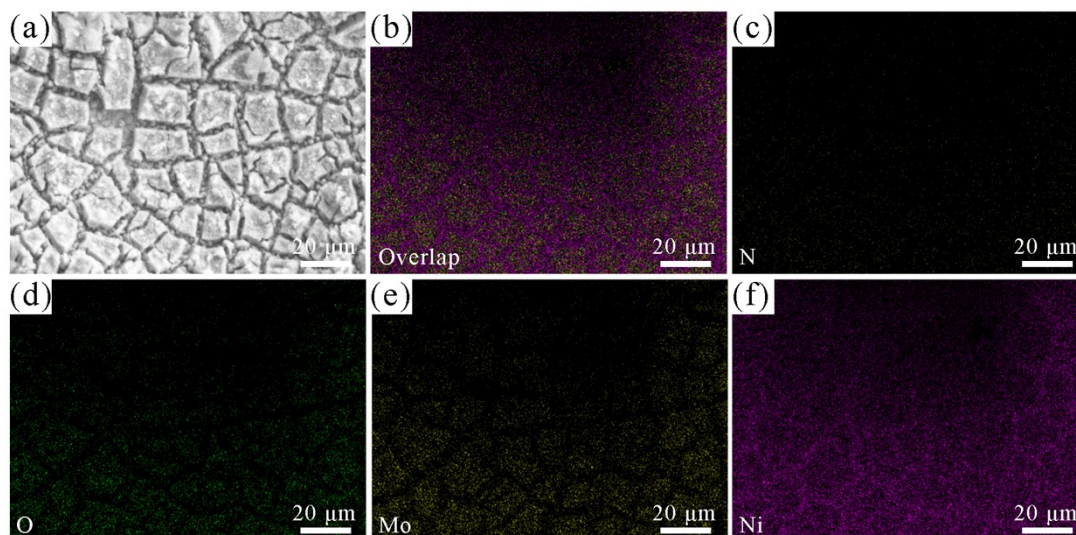
Figure S15 a-f) SEM image and corresponding EDS mapping of NN/MN/NF after 108 h stability test in 1 M KOH.
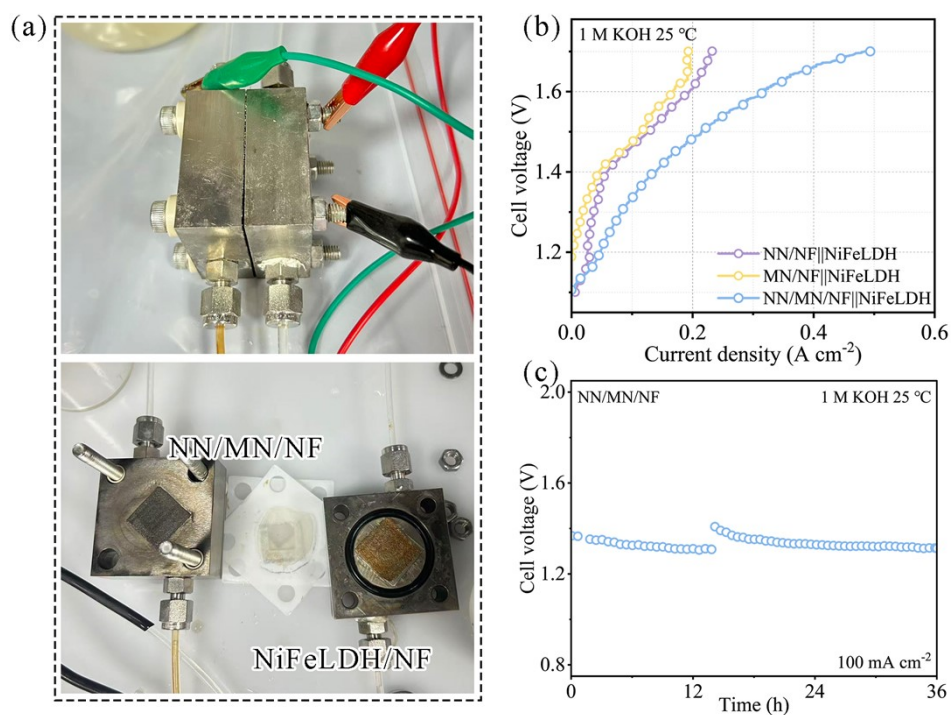
Figure S16 a) Photograph of AEM electrolyzer. b) LSV curves of overall electrolysis in AEM electrolyzer. c) Stability test of overall electrolysis in AEM electrolyzer.
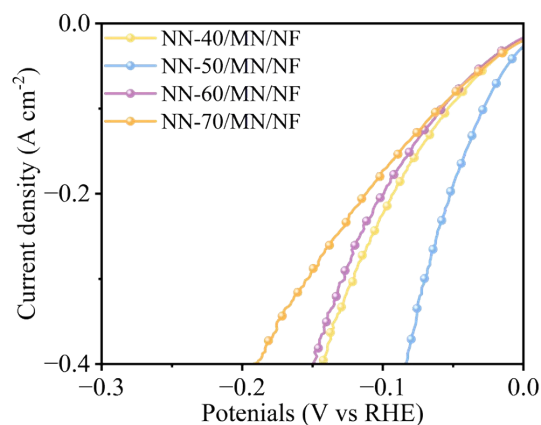
Figure S17 Polarization curves of NN-40/MN/NF, NN-50/MN/NF, NN-60/MN/NF and NN-70/MN/NF in 1 M KOH natural seawater.
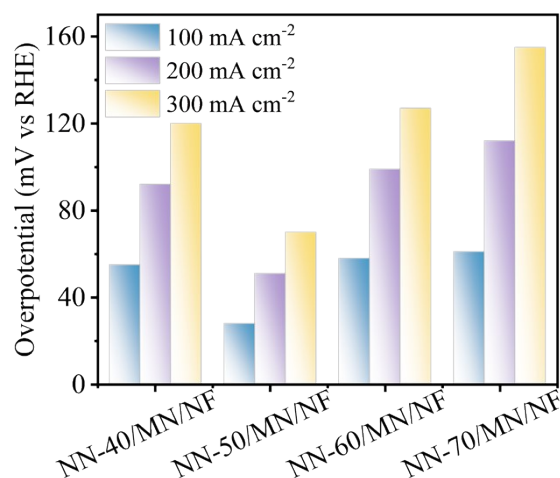
Figure S18 Comparison of the current densities of NN-40/MN/NF, NN-50/MN/NF, NN-60/MN/NF and NN-70/MN/NF at various overpotentials in 1 M KOH natural seawater.
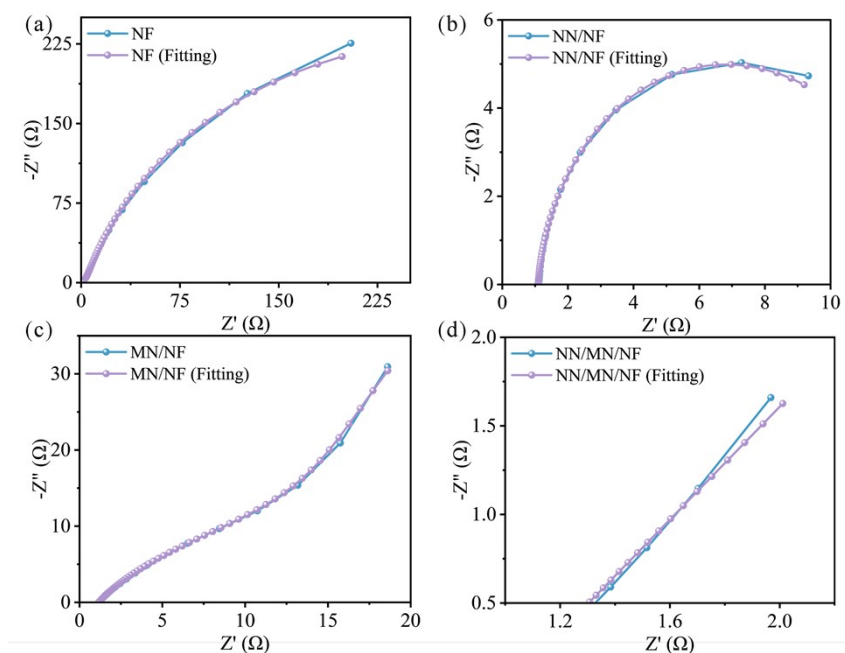
Figure S19 EIS fitting curves of a) NF. b) NN/NF. c) MN/NF. d) NN/MN/NF in 1 M KOH natural seawater.
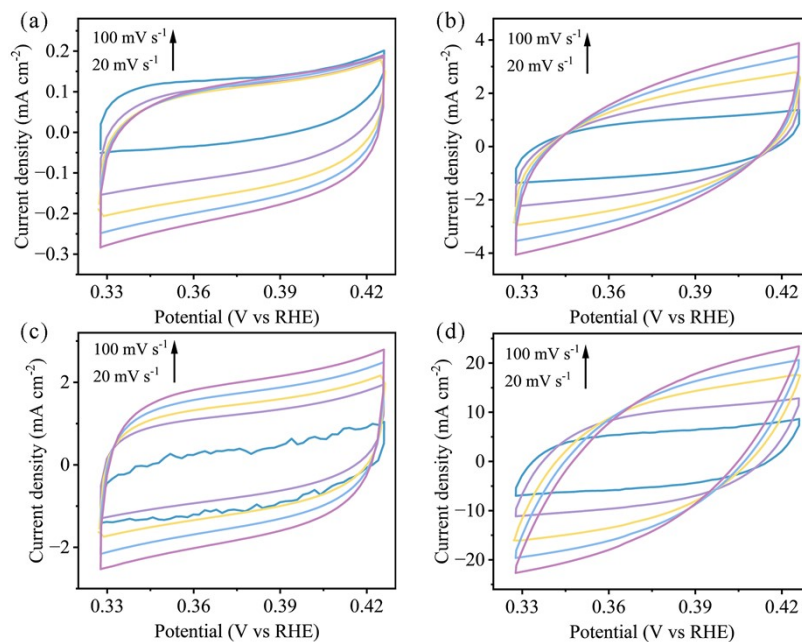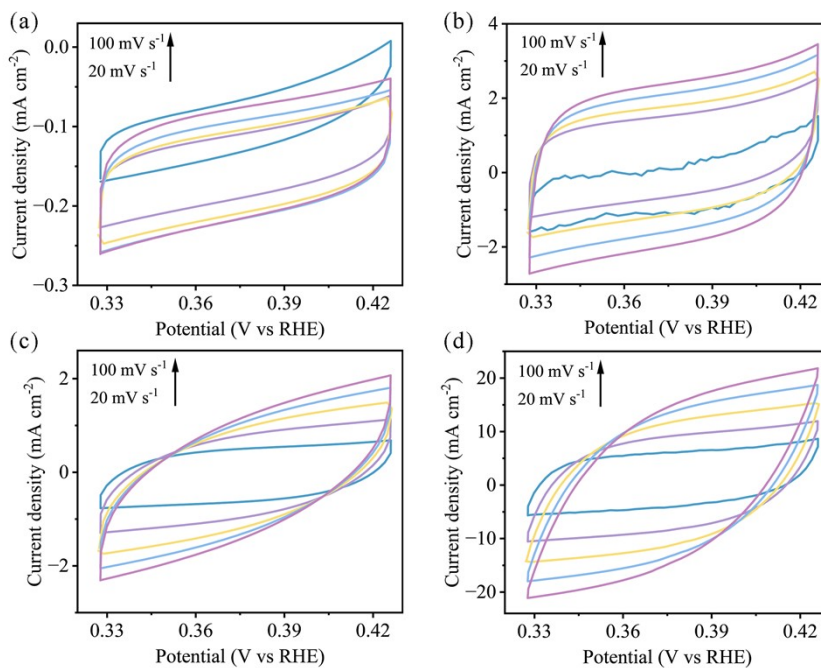
Figure S20 CV curves of a) NF. b) NN/NF. c) MN/NF. d) NN/MN/NF in 1 M KOH natural seawater at 0.33-0.43 V vs RHE with the non-Faradaic potential regions from 10-50 mV s^{-1}.
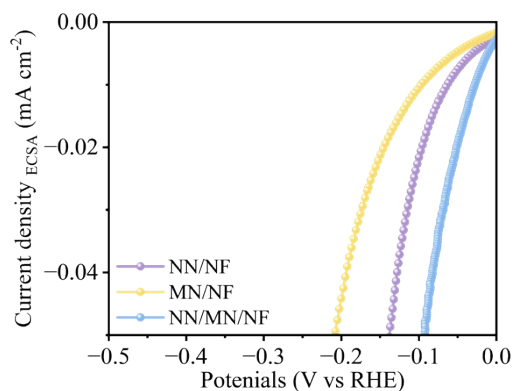

Figure S21 The ECSA-normalized LSV curves of NN/MN/NF and references in 1 M KOH natural seawater.
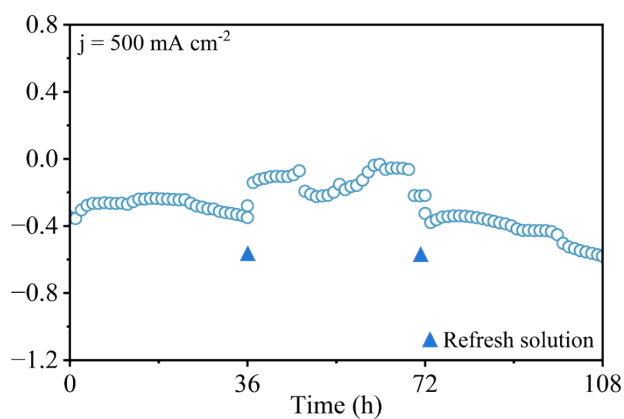
Figure S22 Stability test of the NF in 1 M KOH + seawater.
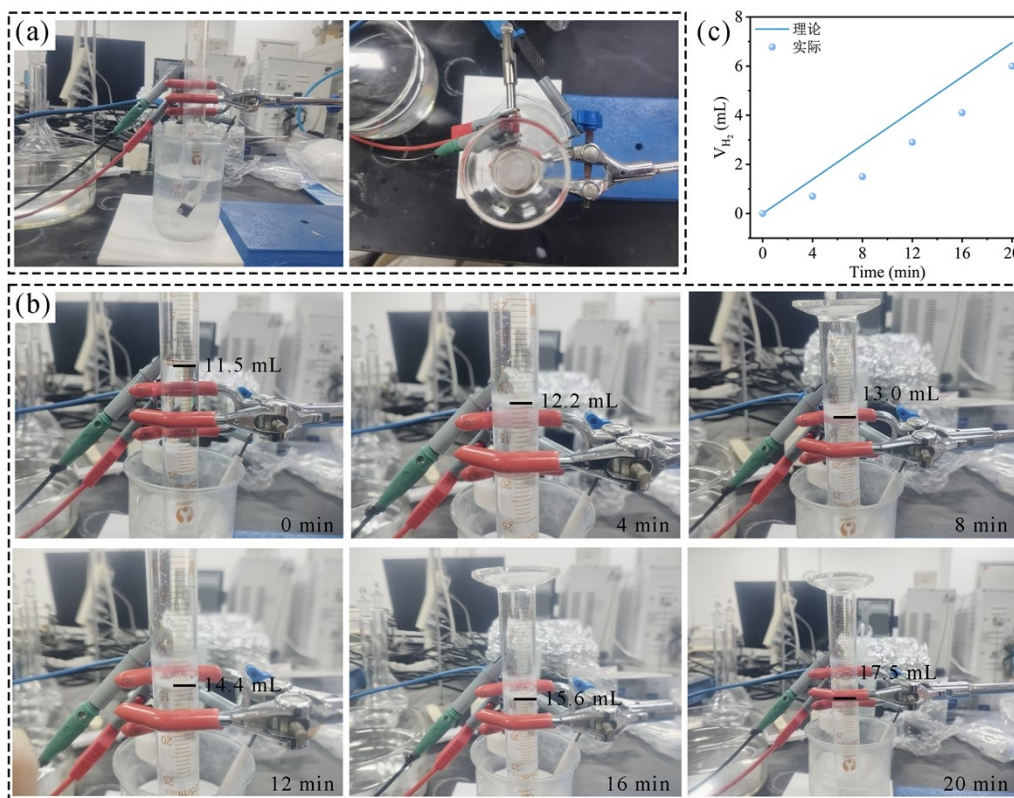
Figure S23 a) Photograph of the home-made setup for measuring H2 volumetric. b) Photograph of gas volume variation over time in 1 M KOH natural seawater at -50 mA cm-2 (240 s intervals) for assessing Faradaic efficiency. c) The measured amount of H2 with different time.
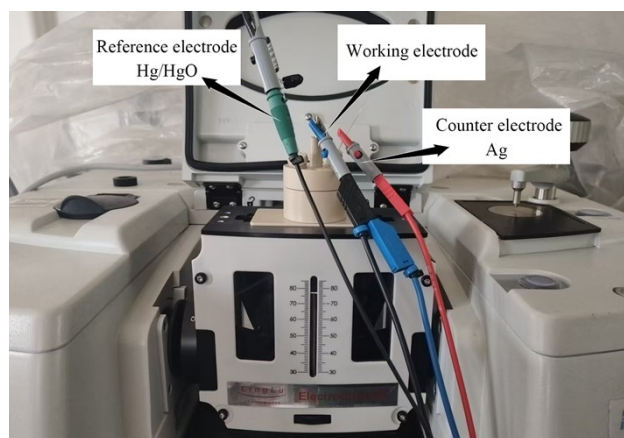
Figure S24 Photograph of the set-up for in situ SEIRAS measurements.
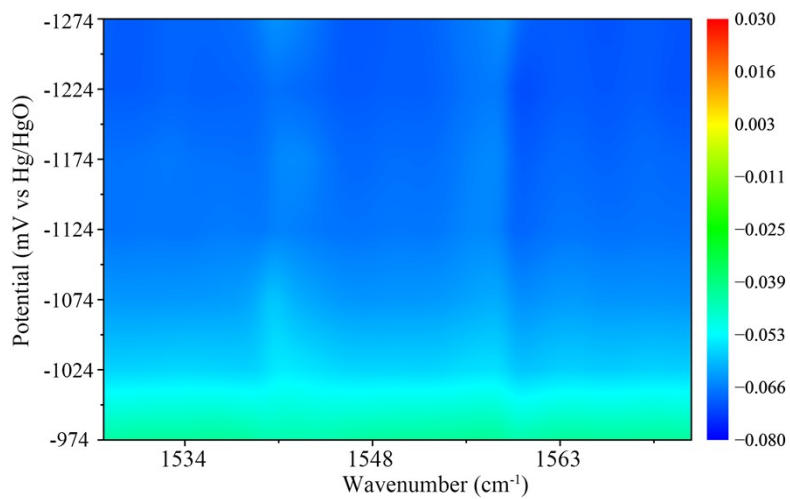
Figure S25 The in situ SEIRAS spectra recorded at potentials from -0.05 to -0.35 V vs Hg/HgO on NF in 1 M KOH natural seawater.
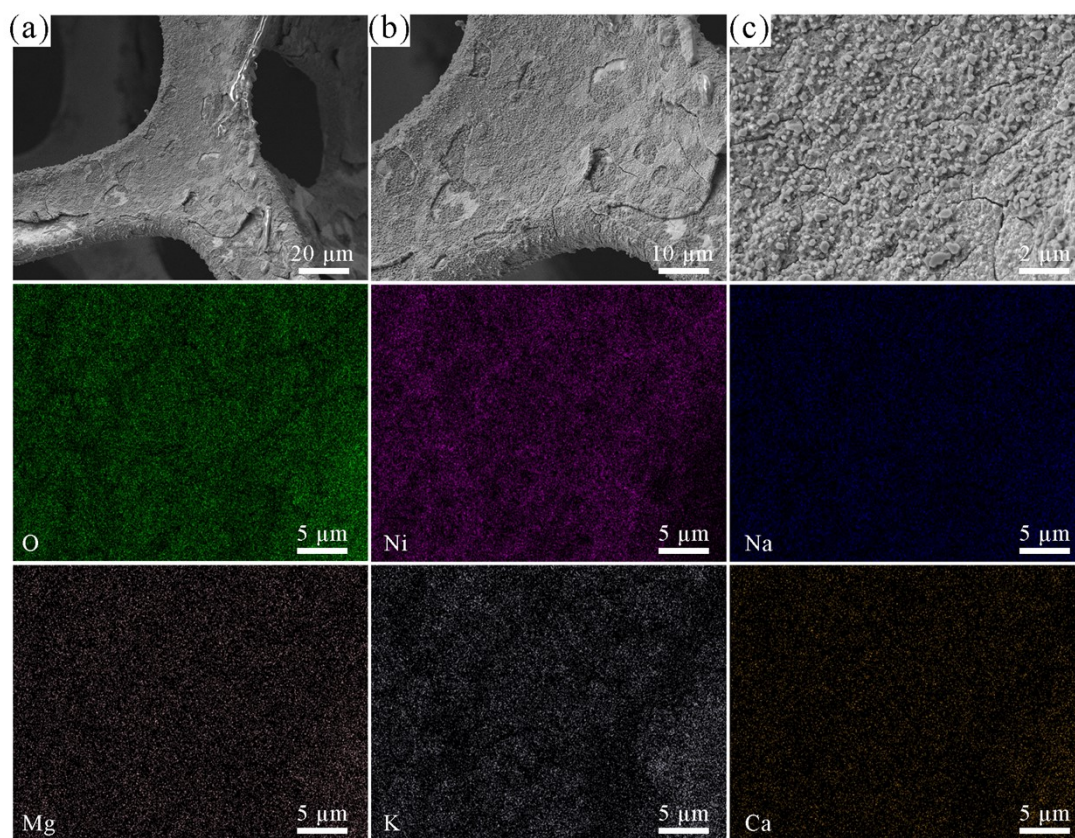
Figure S26 a-c) SEM images and EDS mapping of NF after 108 h stability test in 1 M KOH natural seawater.
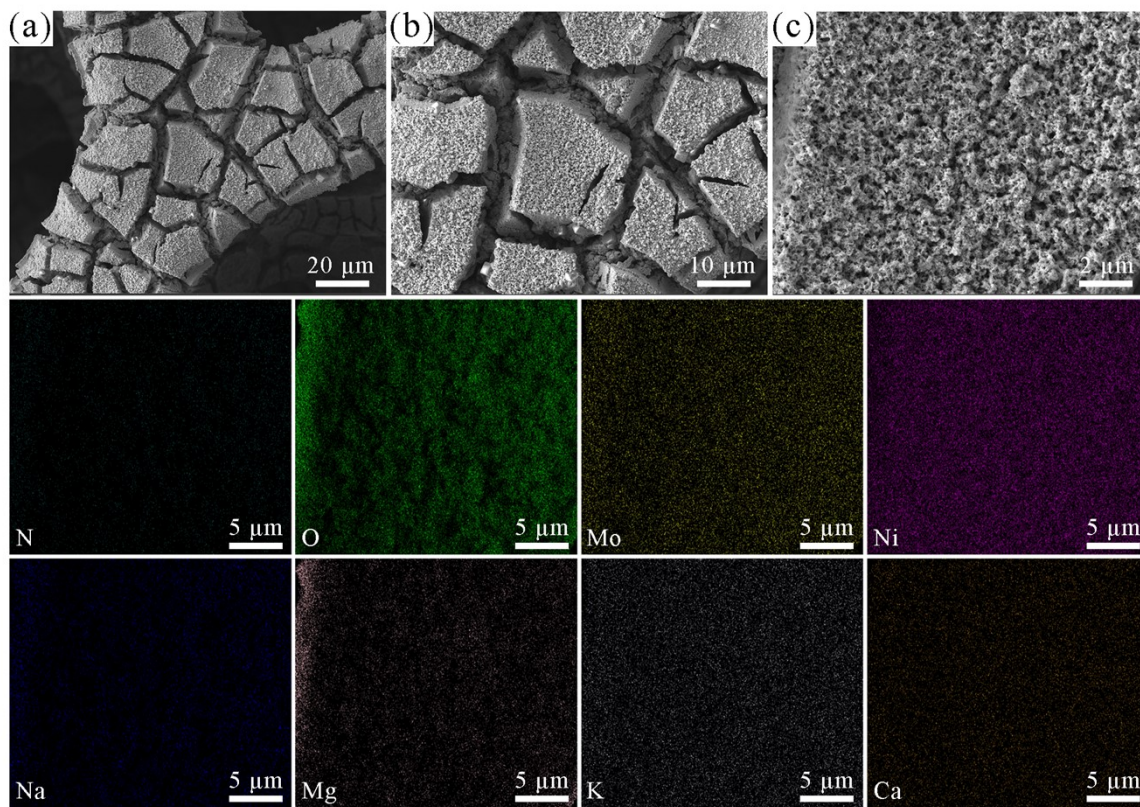
Figure S27 a-c) SEM images and EDS mapping of NN/MN/NF after 108 h stability test in 1 M KOH natural seawater.
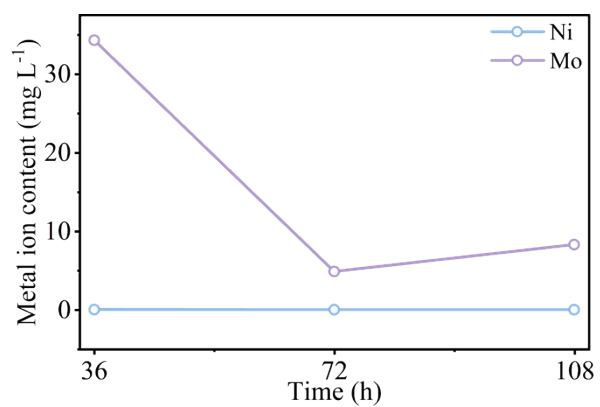
Figure S28 ICP-OES test in 1 M KOH natural seawater.
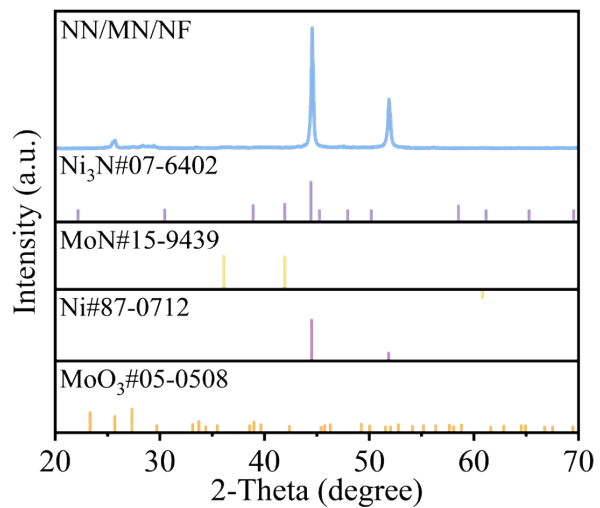
Figure S29 The XRD pattern of NN/MN/NF after 108 h stability test in 1 M KOH natural seawater.

Table S1 The loading mass of fabricated catalysts.

Catalysts	Active sites number (mol cm^{-2})	Loading mass (mg cm^{-2})
NN/NF	$6.57 \times e^{-5}$	36.9
MN/NF	$4.40 \times e^{-5}$	2.5
NN/MN/NF	$3.07 \times e^{-4}$	40.3

Note: The weight of all samples was obtained by subtracting NF mass (Average mass: 51.6 mg cm^{-2}).

Table S2 Comparison with the catalytic activity of the NN/MN to the other recently reported HER catalysts in alkaline solution.

Catalysts	Substrates	Overpotential (mV) @500 mA cm^{-2}	Reference
This work	Nickel foam	106	This work
Ni(OH)x/Ni$_3$S$_2$	Nickel foam	193	Small. 2023, 19, 202205719[1]
F-Co$_2$P/Fe$_2$P	Iron foam	229.8	Chem. Eng. J. 2020, 399, 125831[2]
MoS$_2$/Ni$_3$S$_2$	Nickel foam	182	Sci. Bull. 2020, 65, 123-130[3]
CoNi@CN-CoNiMoO	Nickel foam	168	Carbon Energy. 2023, 5, 22162004[4]
Mo-Ni$_2$P@Ni1$_2$P$_5$-V$_p$	Nickel foam	172	Adv. Mater. 2025, 37, 202502523[5]
Pt-SAs/ac-NiFe LDH	Nickel foam	97	J. Energy Chem. 2025, 107, 427-439[6]
(FeMnMoNi)Se$_2$	Nickel foam	130.5	Chem. Eng. J. 2025, 511, 162264[7]
PMoNiTm	Nickel foam	101.9	Chem. Eng. J. 2025, 508, 160921[8]
FeCoP/TiN	Carbon paper	129	Adv. Funct. Mater. 2025, 202505078[9]
Ru SAs@NiCoP	Nickel foam	240	*Adv. Energy Mater.* 2025, 202501995[10]

Table S3 EIS analysis of different samples in 1 M KOH natural seawater.

Sample	R_s (Ω)	R_{ct} (Ω)	Overall error (%)
NF	1.14	595	1.62
NN/NF	1.08	0.0179	1.78
MN/NF	1.16	146	1.32
NN/MN/NF	0.99	0.00124	1.06

Rs: Solution resistance.   Rct: Charge transmission resistance.

Table S4 Comparison with the catalytic activity of the NN/MN to the other recently reported alkaline seawater HER catalysts.

Catalysts	Substrates	Overpotential (mV) @500 mA cm^{-2}	Tafel (mV dec^{-1})	Reference
This work	Nickel foam	96	55.30	This work
RuMo/Cu$_2$O@C	Copper foam	178	49.90	Adv. Mater. 2025, 2416658[11]
CN@NiCoS	Nickel foam	193.2	60.70	Nat. Commun. 2024, 15, 6154[12]
CoFeOF	Nickel foam	340	90.43	Chem. Eng. J. 2024, 480, 146545[13]
MnCo/NiSe	Nickel foam	216.3	58.24	Appl. Catal. B-Environ. Energy. 2023, 325, 122355[14]
Mo$_2$N/FeO$_x$N$_y$	Nickel foam	550	213	Chem. Eng. J. 2024, 489, 151348[15]
Ni-MoN	Copper foam	128	36.8	Adv. Mater. 2022, 34, 2201774[16]
Ru-CoP$_2$	Nickel foam	152	111.3	J. Energy Chem. 2025, 100, 317-326[17]
Os-Ni$_4$Mo/MoO$_2$	Nickel foam	113	38.5	Adv. Energy Mater. 2024, 14, 2400975[18]
Fe$_2$P/Ni$_{1.5}$Co$_{1.5}$N/Ni$_2$P	Nickel foam	141	43.4	ACS Nano. 2023, 17, 1681-1692[19]
F-FeCoP$_v$	Iron foam	180	108	Appl. Catal. B Environ. 2023, 328, 122487[20]
NC/Ni$_3$Mo$_3$N	Nickel foam	350	39.9	Appl. Catal. B

				Environ. 2020, 272, 118956[21]
NiMoO$_x$/NiMoS	Nickel foam	174	89	Nat. Commun. 2020, 11 (1), 5462[22]
NiMoN	Nickel foam	160	45.6	Nat. Commun. 2019, 10, 5106[23]
Ni$_2$P-Fe$_2$P	Nickel foam	340	86	Adv. Funct. Mater. 2021, 31, 2006484[24]
NiPS	Nickel foam	391	89	J. Energy Chem. 2022, 75, 66-73[25]
NiS@FeNiP	Nickel foam	237	61.9	Small 2023, 19, 2300194[26]
NiFeP/Ni$_2$S$_3$	Nickel foam	406	36.1	Appl. Catal. B Environ. Energy. 2024, 352, 124028[27]
B-Ni$_2$P-MoO$_2$	Nickel foam	157	56	J. Phys. Chem. Lett. 2023, 14, 7264-7273[28]
NiCoP foam	Nickel foam	262	21.88	J. Mater. Chem. A. 2024, 12, 2680-2684[29]

Table S5 EDS analysis after durability test in alkaline natural seawater.

Electrode	Element	Weight (%)	Atomic (%)
NF	O	23.3	46.1
	Ni	57.1	30.8
	Na	9.5	13.1
	Mg	3.9	5.0
	K	5.0	4.0
	Ca	1.3	1.0
	N	0.1	0.2
NN/MN/NF	O	22.8	50.5
	Mo	4.9	1.8
	Ni	65.0	39.2
	Na	1.1	1.8
	Mg	1.7	2.6
	K	2.7	2.4
	Ca	1.6	1.5

Table S6 Concentrations of metal elements after reaction in 1 M KOH natural seawater by ICP-OES (36 h intervals).

Electrolyte Solution		ICP-OES content of metal in electrolyte solution, mg/L		
		36 h	72 h	108 h
1 M KOH natural seawater	Ni	0.0148	0.0058	0.0031
	Mo	34.3222	4.8615	8.2956

[1] W. He, R. Zhang, D. Cao, Y. Li, J. Zhang, Q. Hao, H. Liu, J. Zhao, H.L. Xin, Super-hydrophilic microporous $Ni(OH)_x/Ni_3S_2$ heterostructure electrocatalyst for large-current-density hydrogen evolution, Small 19 (2023) 2205719.

[2] X.-Y. Zhang, Y.-R. Zhu, Y. Chen, S.-Y. Dou, X.-Y. Chen, B. Dong, B.-Y. Guo, D.-P. Liu, C.-G. Liu, Y.-M. Chai, Hydrogen evolution under large-current-density based on fluorine-doped cobalt-iron phosphides, Chem. Eng. J. 399 (2020) 125831.

[3] S. Xue, Z. Liu, C. Ma, H.-M. Cheng, W. Ren, A highly active and durable electrocatalyst for large current density hydrogen evolution reaction, Sci. Bull. 65 (2020) 123–130.

[4] G. Qian, J. Chen, W. Jiang, T. Yu, K. Tan, S. Yin, Strong electronic coupling of CoNi and N-doped-carbon for efficient urea-assisted H_2 production at a large current density, Carbon Energy 5 (2023) e368.

[5] S. Fan, G. Yang, Y. Jiao, Y. Liu, J. Wang, H. Yan, H. Fu, Doping Mo triggers charge distribution optimization and P vacancy of $Ni_2P@Ni_{12}P_5$ heterojunction for industrial electrocatalytic production of adipic acid and H_2, Adv. Mater. 37 (2025) 2502523.

[6] B. Wang, Z. Luo, H. Sun, M. Chen, Y. Zhang, X. Zhao, G. Qiu, B. Xiao, T. Zhou, Q. Lu, D. Li, Y. Wu, Y. Zhang, J. Zhao, J. Zhang, H. Cui, F. Liu, T. He, Q. Liu, Electronic modulation of amorphous/crystalline NiFe LDH by atomic Pt loading enabling industrial hydrogen production in alkaline water and seawater, J. Energy Chem. 107 (2025) 427–439.

[7] Y. Fu, H. Liu, B. Gao, J. Mu, G. Guan, Z. Feng, High-entropy $(FeMnMoNi)Se_2$ nanoflower structure with multi-active sites for urea-assisted hydrogen generation, Chem. Eng. J. 511 (2025) 162264.

[8] T. Zhou, S. Yu, Y. Tang, X. Huang, J.J. Fu, P.K. Shen, Z.Q. Tian, Built-in electric field engineering of MoO_2-Ni heterostructure by P 3p-Mo 4d-Tm 4f orbitals hybridization for efficient industrial-level hydrogen production, Chem. Eng. J. 508 (2025) 160921.

[9] X. Yang, W. Guo, H. Xi, H. Pang, Y. Ma, X. Leng, C. Hou, L. Li, X. Huang, F. Meng, Engineering N-TM(Co/Fe)-P interfacial electron bridge in transition metal phosphide/nitride heterostructure nanoarray for highly active and durable hydrogen evolution in large-current seawater electrolysis, Adv. Funct. Mater. (2025) 2505078.

[10]J. Fan, J. Xia, H. Wang, H. Li, Y. Tao, G. Wang, W. Hao, Q. Bi, G. Li, X. Shen, L. Ai, Unveiling the role of single atomic ruthenium decorated cactus-like bimetallic phosphides for alkaline water electrolysis, Adv. Energy Mater. 15 (2025) 2501995.

[11]X. Yang, H. Shen, X. Xiao, Z. Li, H. Liang, S. Chen, Y. Sun, B. Jiang, G. Wen, S. Wang, L. Zhang, Regulating interfacial H_2O activity and H_2 bubbles by core/shell nanoarrays for 800 h stable alkaline seawater electrolysis, Adv. Mater. Xxx (2025) 2416658.

[12]M. Li, H. Li, H. Fan, Q. Liu, Z. Yan, A. Wang, B. Yang, E. Wang, Engineering interfacial sulfur migration in transition-metal sulfide enables low overpotential for durable hydrogen evolution in seawater, Nat. Commun. 15 (2024) 6154.

[13]S.A. Patil, A.C. Khot, V.D. Chavan, I. Rabani, D. Kim, J. Jung, H. Im, N.K. Shrestha, Electrostatically robust CoFeOF nanosheet against chloride for green-H_2 production in alkaline seawater electrolysis, Chem. Eng. J. 480 (2024) 146545.

[14]Y. He, Y. Hu, Z. Zhu, J. Li, Y. Huang, S. Zhang, M.-S. Balogun, Y. Tong, High-performance multidimensional-structured N-doped nickel modulated Mo_2N/FeO_xN_y bifunctional electrocatalysts for efficient alkaline seawater splitting, Chem. Eng. J. 489 (2024) 151348.

[15]R. Andaveh, A. Sabour Rouhaghdam, J. Ai, M. Maleki, K. Wang, A. Seif, G. Barati Darband, J. Li, Boosting the electrocatalytic activity of NiSe by introducing MnCo as an efficient heterostructured electrocatalyst for large-current-density alkaline seawater splitting, Appl. Catal. B Environ. 325 (2023) 122355.

[16]L. Wu, F. Zhang, S. Song, M. Ning, Q. Zhu, J. Zhou, G. Gao, Z. Chen, Q. Zhou, X. Xing, T. Tong, Y.

Yao, J. Bao, L. Yu, S. Chen, Z. Ren, Efficient alkaline water/seawater hydrogen evolution by a nanorod-nanoparticle-structured Ni-MoN catalyst with fast water-dissociation kinetics, Adv. Mater. 34 (2022) 2201774.

[17] B. Deng, J. Shen, J. Lu, C. Huang, Z. Chen, F. Peng, Y. Liu, Ru doping triggering reconstruction of cobalt phosphide for coupling glycerol electrooxidation with seawater electrolysis, J. Energy Chem. 100 (2025) 317–326.

[18] L. Guo, J. Chi, T. Cui, J. Zhu, Y. Xia, H. Guo, J. Lai, L. Wang, Phosphorus defect mediated electron redistribution to boost anion exchange membrane-based alkaline seawater electrolysis, Adv. Energy Mater. 14 (2024) 2400975.

[19] F. Zhang, Y. Liu, F. Yu, H. Pang, X. Zhou, D. Li, W. Ma, Q. Zhou, Y. Mo, H. Zhou, Engineering multilevel collaborative catalytic interfaces with multifunctional iron sites enabling high-performance real seawater splitting, ACS Nano 17 (2023) 1681–1692.

[20] J. Zhu, J. Chi, T. Cui, L. Guo, S. Wu, B. Li, J. Lai, L. Wang, F doping and P vacancy engineered FeCoP nanosheets for efficient and stable seawater electrolysis at large current density, Appl. Catal. B Environ. 328 (2023) 122487.

[21] Y. Chen, J. Yu, J. Jia, F. Liu, Y. Zhang, G. Xiong, R. Zhang, R. Yang, D. Sun, H. Liu, W. Zhou, Metallic Ni_3Mo_3N porous microrods with abundant catalytic sites as efficient electrocatalyst for large current density and superstability of hydrogen evolution reaction and water splitting, Appl. Catal. B Environ. 272 (2020) 118956.

[22] P. Zhai, Y. Zhang, Y. Wu, J. Gao, B. Zhang, S. Cao, Y. Zhang, Z. Li, L. Sun, J. Hou, Engineering active sites on hierarchical transition bimetal oxides/sulfides heterostructure array enabling robust overall water splitting, Nat. Commun. 11 (2020) 5462.

[23] L. Yu, Q. Zhu, S. Song, B. McElhenny, D. Wang, C. Wu, Z. Qin, J. Bao, Y. Yu, S. Chen, Z. Ren, Non-noble metal-nitride based electrocatalysts for high-performance alkaline seawater electrolysis, Nat. Commun. 10 (2019) 5106.

[24] L. Wu, L. Yu, F. Zhang, B. McElhenny, D. Luo, A. Karim, S. Chen, Z. Ren, Heterogeneous bimetallic phosphide Ni_2P-Fe_2P as an efficient bifunctional catalyst for water/seawater splitting, Adv. Funct. Mater. 31 (2021) 2006484.

[25] H.-Y. Wang, J.-T. Ren, L. Wang, M.-L. Sun, H.-M. Yang, X.-W. Lv, Z.-Y. Yuan, Synergistically enhanced activity and stability of bifunctional nickel phosphide/sulfide heterointerface electrodes for direct alkaline seawater electrolysis, J. Energy Chem. 75 (2022) 66–73.

[26] J. Ren, L. Chen, W. Tian, X. Song, Q. Kong, H. Wang, Z. Yuan, Rational synthesis of core-shell-structured nickel sulfide-based nanostructures for efficient seawater electrolysis, Small 19 (2023) 2300194.

[27] Y. Song, X. Zhang, Z. Xiao, Y. Wang, P. Yi, M. Huang, L. Zhang, Coupled amorphous NiFeP/cystalline Ni_3S_2 nanosheets enables accelerated reaction kinetics for high current density seawater electrolysis, Appl. Catal. B Environ. Energy 352 (2024) 124028.

[28] L.P. Phan, T.T.N. Tran, T.-K. Truong, J. Yu, H.-V.T. Nguyen, T.B. Phan, N.H. Thi Tran, N.Q. Tran, Highly efficient and stable hydrogen evolution from natural seawater by boron-doped three-dimensional Ni_2P–MoO_2 heterostructure microrod arrays, J. Phys. Chem. Lett. 14 (2023) 7264–7273.

[29] L. He, Z. Cai, D. Zheng, L. Ouyang, X. He, J. Chen, Y. Li, X. Guo, Q. Liu, L. Li, W. Chu, S. Zhu, X. Sun, B. Tang, Three-dimensional porous NiCoP foam enabled high-performance overall seawater splitting at high current density, J. Mater. Chem. A 12 (2024) 2680–2684.